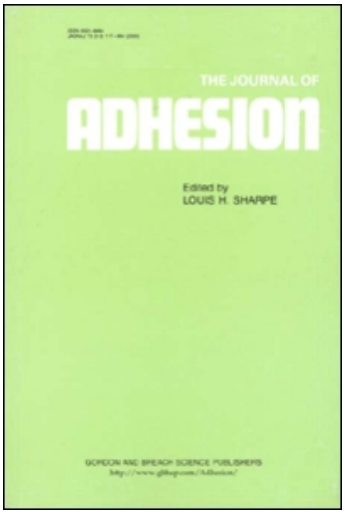

The Journal of Adhesion
Publication details, including instructions for authors and subscription information:
http://www.informaworld.com/smpp/title~content=t713453635

Strain energy release rates of a pressure sensitive adhesive measured by the shaft-loaded blister test

E. P. O'Brien[a]; T. C. Ward[b]; S. Guo[c]; D. A. Dillard[c]
[a] Department of Chemical Engineering, Virginia Tech, Blacksburg, Virginia, USA [b] Department of Chemistry, Virginia Tech, Blacksburg, Virginia, USA [c] Engineering Science and Mechanics Department, Virginia Tech, Blacksburg, Virginia, USA

Online publication date: 08 September 2010

To cite this Article O'Brien, E. P. , Ward, T. C. , Guo, S. and Dillard, D. A.(2003) 'Strain energy release rates of a pressure sensitive adhesive measured by the shaft-loaded blister test', The Journal of Adhesion, 79: 1, 69 — 97
To link to this Article: DOI: 10.1080/00218460309560
URL: http://dx.doi.org/10.1080/00218460309560

The Journal of Adhesion, 79: 69–97, 2003

0021-8464/03 $12.00 +.00
DOI: 10.1080/00218460390147924

Taylor & Francis
Taylor & Francis Group

STRAIN ENERGY RELEASE RATES OF A PRESSURE SENSITIVE ADHESIVE MEASURED BY THE SHAFT-LOADED BLISTER TEST

E. P. O'Brien
Department of Chemical Engineering,
Virginia Tech, Blacksburg,
Virginia, USA

T. C. Ward
Department of Chemistry,
Virginia Tech, Blacksburg,
Virginia, USA

S. Guo and D. A. Dillard
Engineering Science and Mechanics Department,
Virginia Tech,
Blacksburg,
Virginia, USA

The elastic solution to the shaft-loaded blister test (SLBT) was adopted to measure the applied strain energy release rate (G) of Kapton® pressure sensitive adhesive (PSA) tape bonded to a rigid substrate. The substrates used were either aluminum or Teflon®, a high-energy surface and low-energy surface, respectively. The values of G were calculated from three different equations: (1) load-based, (2) hybrid, and (3) displacement-based. An experimental compliance calibration was utilized to measure the film's effective tensile rigidity, $(Eh)_{eff}$, the results of which are

Received 1 March 2002; in final form 19 July 2002.

The authors would like to acknowledge the financial support of the Center for Adhesive and Sealant Science at Virginia Tech and the Adhesive and Sealant Council Education Foundation. The authors would also like to thank Dr. Kai-tak Wan for his helpful suggestions and Dr. Taigyoo Park of Polymer Solutions, Inc. for assistance in the earliest stage of this work. We would also like to thank the Pressure Sensitive Tape Council who helped sponsor the presentation of this material at their 23rd Annual Technical Seminar, 2000.

Presented at the 24th Annual Meeting of The Adhesion Society, Inc., held at Williamsburg, Virginia, USA, 25–28 February 2001.

Address correspondence to Thomas C. Ward, Department of Chemistry, 2107 Hahn Hall (0344), Virginia Tech, Blacksburg, VA 24061, USA. E-mail: tward@vt.edu

presented in an appendix. Plastic deformation at the contact area of the shaft tip and adhesive results in an overestimated displacement (w_0) (relative to the elastic model), leading to disagreement among the values of G calculated. Estimation of the effective membrane stress in the film, (N_{eff}), as well as the reasonable agreement between the value of (Eh) determined from a stress-strain experiment and the compliance calibration, suggest that, in spite of the plastic deformation, the assumption of linear elasticity in the crack growth region and hence the validity of the model, is reasonable. The compliance calibration has been shown to improve the agreement among the values of G calculated from the three equations. Using the load-based equation, the assumed "correct" value of G may be obtained for a thin adhesive coating independent of the film's stiffness even in the presence of plastic deformation at the shaft tip. Comparing the value of G obtained by a pull-off test and the 90° peel test for a single ply indicates that the value of G obtained by the SLBT is of reasonable magnitude, being less than that obtained by the more firmly established pull-off test, and also that undesirable plastic deformation is reduced relative to the 90° peel test. An experimental configuration for studying the effects of liquids on the fracture energy has been demonstrated for the SLBT. This study indicates that the SLBT is an attractive and convenient test method for measuring the strain energy release rate of adhesive films, because of the insensitivity of the load-based equation to the coating stiffness, plus the independence of the value of G on the plastic deformation at the shaft tip, and the reduced plastic deformation at the crack front relative to the 90° peel.

Keywords: Strain energy release rate; Pressure sensitive adhesive tapes; Shaft-loaded blister test; Pull-off test; Peel test; Plastic deformation; Environmental degradation; Kapton®

INTRODUCTION

Measuring the adhesion of many important thin coatings is difficult given their small load-bearing capacity, associated with the thinness, and their relatively strong adhesion [1]. These conditions often lead to the film rupturing before debonding can occur. Even if film rupturing is absent and delamination is successful, significant plastic deformation of the film may result. In this case, calculations of the fracture toughness of the adhesive bond, or the applied strain energy release rate (G), may not reflect the intrinsic adhesion strength due to the additional energy consumed by the bending and stretching of the adhesive coating. For example, Kim et al. [2] has reported that measured peel forces may be 100 times greater than the actual adhesion strength.

Thin adhesive coatings can be conveniently tested using the peel geometry. For a linear elastic coating of large tensile stiffness and small bending stiffness, the strain energy release rate can be expressed as follows [3]:

$$G = \frac{P}{b}(1 - \cos\theta) \tag{1}$$

where b is the width of the film, P is the load, and θ is the angle between the peel arm and the substrate. In practice, the peel force also depends on plastic dissipation within the coating, which is a function of the angle (or geometry) and stiffness and/or thickness of the peel arm along with the resulting stresses generated during bending and stretching the film. As a consequence, Equation (1) has little utility beyond comparing the adhesion of nominally identical films loaded in identical fashion [4]. Gent and Kaang [5] have observed higher strain energy release rates obtained from the 180° peel test relative to the 90° peel test due to larger bending stresses. Conversely, at small peel angles significant energy is stored due to the tensile stresses and stretching of the film. Gent and Kaang suggest using an angle of 45° and limiting the tensile strain to below 10–15%; under their conditions, less than a 20% increase in the peel force resulted, compared with the extrapolated intrinsic adhesive strength.

Film rupture during peel testing can occur not only from the high stresses generated but also from the use of mechanical grips. A typical solution is to employ a backing or reinforcement layer to strengthen the adhesive coating; however, the additional reinforcement can change the stiffness of the peel arm and the subsequent peel force. Gent and Hamed [6] showed that for very thin films of Mylar®, which yield substantially during peeling, as the adhesive coating thickness increased the peel force also rose due to an increase in the strain energy. However, a further increase in the thickness showed that the peel forces were reduced as the stiffness of the film increased. This latter effect was attributable to an increase in yield stress of the film and a reduction in bending stresses, which is consistent with what was shown by Kim et al. [2]. A critical thickness was observed beyond which no further change in the peel force was observed as the thickness was increased.

Given that the peel force and corresponding value of G depend on the energy consumed during plastic deformation of the adhesive, efforts have been made to determine an intrinsic adhesive fracture energy by considering the energy dissipated during tensile deformation and bending of the peel arm in addition to the energy stored in the peel arm. Kinloch et al. [7] utilized this approach to calculate G_a, a "geometry independent" parameter, independent of the peel angle and thickness of the adhesive. Moidu et al. [8, 9] developed an analytic approach to determine the plastic deformation in the adhesive and also studied the effects of constitutive properties of the adhesive and peel angle.

Ideally, for thin coatings an adhesion test should reduce the above discussed misleading effects of the angle and stiffness of the peel arm, reduce plastic deformation, and eliminate the use of mechanical grips. In addition, a procedure for reinforcing the film without significantly affecting the measured peel force would be beneficial. A test that, in general, meets these requirements is the pull-off test [10], or V-peel test [11], illustrated in Figure 1. In this experiment, to initiate debonding a force is applied by a pin that is placed perpendicular to and in the center of a strip of coating. From the peel force and angle of debond the strain energy release rate can be determined from Equation (2):

$$G_c = \frac{3}{8}\frac{P\theta}{b} \tag{2}$$

Gent and Kaang [10] showed that the value of G_c obtained from the pull-off test was independent of the film stiffness. The value of G_c was also significantly less than that obtained by the 90° peel test due to the small angle of deflection between the peel arm and substrate ($< 25°$), which led to a decrease in the plastic deformation arising from bending stresses.

Another broad category of tests that eliminates the use of grips and reduces plastic deformation due to bending (due to the small angle between the peel arm and substrate) are the blister tests. Blister specimens consist of a thin film adhered to a substrate that has a hole in its center. The development of the first blister test is credited to Dannenburg [12]. However, it was not until the work of Williams [13] that the circular blister geometry was adopted. In the standard or pressurized circular blister test, either a liquid or gas is pressurized through the hole against the underside of the coating until a blister

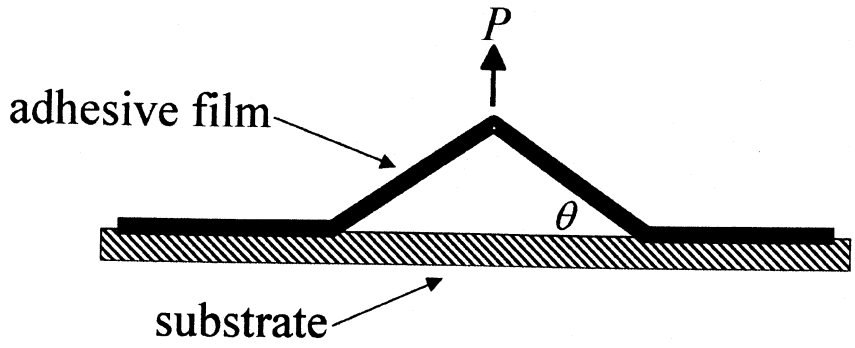

FIGURE 1 Schematic of the pull-off test.

crack is formed. The strain energy release rate can be calculated from the relationship between the pressure, blister radius, and blister height. Similar to the pull-off test, it has been shown that the strain energy release rate for the blister test is independent of the stiffness of the film and specimen geometry [14]. However, a disadvantage of the standard blister is that the strain energy release rate increases as the blister radius increases, which could lead to uncontrolled catastrophic debonding [1]. To circumvent the problem of uncontrolled failure, a constant strain energy release rate test—the "constrained blister"—was proposed by Chang et al. [15] and Napolitano et al. [16]. Allen and Senturia [17, 18] proposed an "island blister" test to reduce stresses on the film, enabling high strain energy release rates at relatively low pressures; however, a drawback of the island blister is that uncontrolled debonding can still occur. Dillard and Bao [19] extended this to an additional constant strain energy release rate test, the "peninsula blister". Wan and Breach [20] and Wan [21] also developed a blister test that eliminates catastrophic debonding by utilizing a fixed amount of the pressurizing gas, where the increase in pressure is driven thermally.

The blister test geometry also has a number of advantages when used for testing adhesives subjected to environmental stress (time, temperature, and fluid). Specimens where the adhesive is sandwiched between two impermeable adherends expose only an edge to the environment, increasing the time necessary to saturate the adhesive and degrade the interface. Open face specimens such as peel specimens can considerably reduce the exposure time before deleterious effects of the environment are observed [22, 23]. However, the interfacial degradation may be more pronounced at the sample edge, which can produce misleading results. For such environmental degradation tests, blister specimens have several advantages: (1) the pressurizing medium can be the degrading fluid of choice, (2) the axisymmetric geometry of the blister eliminates edge effects, and (3) direct exposure or diffusion of the fluid occurs perpendicular to the debond front.

In this paper, we explore the shaft-loaded blister test (SLBT) (Figure 2), which utilizes the controlled displacement of a spherically capped shaft, driven by a universal testing machine (UTM), as an alternative to applying fluid or gas media. Malyshev and Salganik [24] were the first to explore this test geometry and derived the strain energy release rate for a pure bending plate boundary condition. Wan and Mai [25] developed an analytic solution to derive the strain energy release rate for a pure stretching elastic film in a conical geometry and provided additional analysis that accounts for plastic yielding at the contact area of the shaft tip. This elastic solution was adopted to

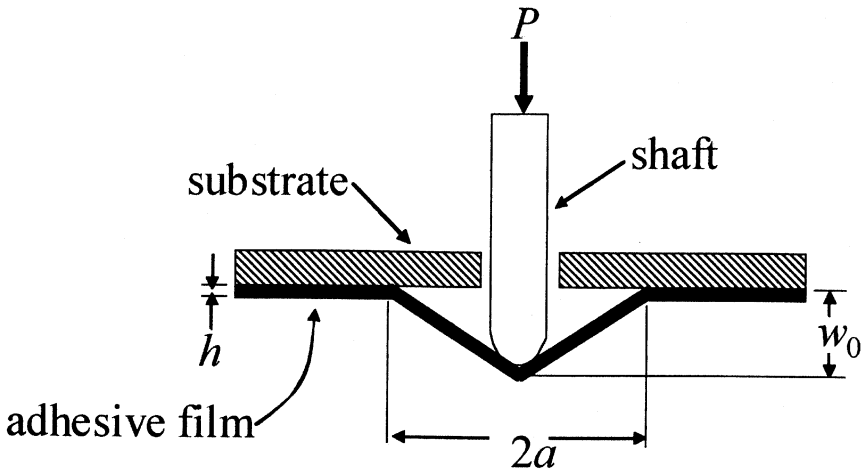

FIGURE 2 Schematic of the shaft-loaded blister test.

measure the adhesion of nylon to aluminum [26]. Wan [27] analyzed the transition from a bending plate to a stretching membrane condition in the SLBT geometry. Wan and Liao [28] also adopted the SLBT for measuring the constitutive properties of thin films from the load versus displacement data prior to debonding.

Utilizing the elastic analytic model proposed by Wan and Mai [25], we have adopted the SLBT in order to investigate the adhesion of Kapton® pressure sensitive adhesive (PSA) tape bonded to a rigid substrate. The substrates reported here are either a low-energy surface (Teflon®) or a substrate with a high-energy surface (aluminum). The model was tested and the effects of plastic deformation of the film were probed by examining the value of G calculated from three different equations, which will be termed (1) load-based, (2) hybrid, and (3) displacement-based. The effect of changing the stiffness of the coating while keeping the actual interfacial adhesion constant was investigated by varying the number of plies of PSA tape bonded to the aluminum substrate. The strain energy release rates obtained by the SLBT for a single-ply film are compared with the more conventional pull-off test and 90° peel test. An experimental compliance calibration method for *in situ* measurement of the mechanical properties of the film was also obtained based upon blister crack growth data; in order to preserve the continuity of the paper, this is discussed in the Appendix. The great utility of the SLBT in environmental exposure testing was demonstrated for several fluids and described below.

SHAFT-LOADED BLISTER TEST THEORY

The analytical solution to the shaft-loaded blister by Wan and Mai [25] is based largely on three assumptions: (1) that the film undergoes pure elastic stretching in the radial and tangential directions or, in other words, no bending occurs; (2) the load is approximated as a point load, which results in a conical blister profile; and (3) the angle between the adhesive and substrate is shallow (less than 25°). Based on these assumptions Wan and Mai first arrived at the following relation:

$$Pa^2 = \left(\frac{\pi(Eh)_{\text{eff}}}{4}\right) w_0^3 \tag{3}$$

where a is the radius of debonding, w_0 is the central shaft displacement, P is the load, E is the Young's tensile modulus, and h is the thickness of the backing. Collectively, (Eh) is commonly referred to as the film's tensile rigidity, which defines the film stiffness. $(Eh)_{\text{eff}}$ is the effective tensile rigidity determined from a compliance calibration. Equation (3) is modified from the original work of Wan and Mai—we take the liberty of replacing (Eh) with $(Eh)_{\text{eff}}$, and also utilize Equation (3) to carry out a compliance calibration. The results from application of Equation (3) are presented and discussed in the Appendix.

Utilizing Equation (3) and an energy balance derived from linear elastic fracture mechanics, Wan and Mai arrive at the following three expressions for the strain energy release rate:

$$G = \left(\frac{1}{16\pi^4 Eh}\right)^{1/3} \left(\frac{P}{a}\right)^{4/3} \tag{4}$$

$$G = \frac{1}{\pi^2 Eh} \left(\frac{P}{w_0}\right)^2 \tag{5}$$

$$G = \frac{Eh}{16} \left(\frac{w_0}{a}\right)^4 \tag{6}$$

During stable crack growth, a, w_0, and P are predicted to increase linearly. From the slope of either P versus a, P versus w_0, or w_0 versus a, the value of G can be calculated from Equations (4), (5), or (6), respectively. Examination of these three equations reveals that the value of G calculated from Equation (4) depends strongly on the measured load (P), and the G calculated from Equation (6) depends strongly on the measured displacement (w_0). The debond radius (a) is eliminated from Equation (5), a hybrid form involving both load and displacement. As a consequence Equations (4), (5), and (6) are referred to as the load-based, hybrid, and displacement-based equations, respectively.

The film's tensile rigidity (Eh) can be determined from either an independent stress-strain experiment or from a compliance calibration with the SLBT fixture. The initial linear relationship of the stress-strain experiment yields the Young's modulus, E. For the PSA tape used in our research, the area and stress are calculated based only on the thickness of the backing (Kapton®), not the soft adhesive layer. The tensile rigidity calculated as described from the stress-strain data is denoted as $(Eh)_{\mathrm{UTM}}$. On the other hand, if the adhesive system closely follows the assumptions of the analytic model, then fitting the experimental data to Equation (3) allows a compliance calibration which will then independently determine the effective tensile rigidity of the film $(Eh)_{\mathrm{eff}}$. We note that a plot of $P\,a^2$ versus ${w_0}^3$ should yield a straight line with a slope equal to $\pi\,(Eh)_{\mathrm{eff}}/4$. For several reasons this effective tensile rigidity $(Eh)_{\mathrm{eff}}$ may be more representative of the adhesive film's mechanical properties than the film's tensile rigidity determined from the Young's modulus and the film thickness, $(Eh)_{\mathrm{UTM}}$. Most importantly, the effective tensile rigidity $(Eh)_{\mathrm{eff}}$ can account for such effects as the difference in loading between the uniaxial stress-strain experiment and the biaxial stress the film experiences in the actual blister test configuration. In addition, the effects of the Poisson ratio, shear loading, anisotropy, as well as the coexistence of bending and stretching stresses, may be significant and could be accounted for by the $(Eh)_{\mathrm{eff}}$ method. Overall, this technique is similar to the compliance method often adopted for the double cantilever beam specimen [29].

To estimate the stress in the adhesive film, the effective membrane stress (N_{eff}), is given by Wan and Mai as:

$$N_{\mathrm{eff}} = (GEh)^{1/2}\left[\left(\log\frac{a}{r}\right)^2 + \frac{3}{4}\right]^{1/2} \tag{7}$$

where r is the radial distance from the center of the blister. Membrane stress is defined as the stress multiplied by the film thickness, therefore N_{eff} is not a "true" stress in the strict sense (load per unit cross-sectional area), but rather a force per unit width. Note that the effective membrane stress may be known also as the stress resultant [1]. N_{eff} is composed of only the radial and tangential stress components of the film and ignores stresses due to bending, which may or may not be significant. If $N_{\mathrm{eff}} \geq \sigma_y\, h$, where σ_y is the adhesive's yield strength, then membrane yielding is predicted to occur. Examination of Equation (7) reveals that in the limit of $r \to 0$ the effective stress approaches infinity; thus, in the center of the blister we expect deviations from simple elastic response. However, application of

Equations (3)–(6) requires that the assumption of linear elasticity holds true at the crack front, where $r = a$ and $N_{\text{eff}} = (3G(Eh)/4)^{1/2}$. In the event that $N_{\text{eff}} \geq \sigma_y h$ at the crack front, the elastic blister equations are invalid. The solution for the case of a thin film experiencing plastic deformation in an inner annulus and an elastic outer annulus also has been developed by Wan and Mai, but it is not discussed here.

EXPERIMENTAL

Materials

The PSA tape utilized in the experiments is Kapton® polyimide film tape with a total thickness of 63.5 μm (2.5 mils). The PSA tape is a bilayer system consisting of a Kapton® backing, which has a thickness of 25.4 μm (1 mil), and a pressure sensitive silicone-based thermosetting adhesive, which has a thickness of 38.1 μm (1.5 mils). The base polymer used in silicone-based PSAs is polydimethylsiloxane (PDMS) [30], which has a glass transition at $-125°$C. The PSA tape was bonded to either aluminum or Teflon®, a high-energy and low-energy surface, respectively. The surface energies of Al_2O_3 and Teflon® are 574 and 19.1 mJ/m^2, respectively [31]. The aluminum surface was treated with a caustic solution and rinsed with acetone prior to application of the PSA tape. The Teflon® surface was also rinsed with acetone prior to application of the PSA tape. The tensile modulus (E) of the Kapton® tape, calculated from ASTM D-882-91 using the cross-sectional area of the sample based on the backing thickness, is roughly $3.05 +/- 0.06$ GPa. The stress-strain curve for the PSA tape is shown in Figure 3, and the yield strength, σ_y, was calculated as $120 +/- 6$ MPa using a bimoduli approximation.

Methods

A 0.8 cm diameter hole was bored into the aluminum and Teflon® substrates. The PSA tape dimensions were 2.54×2.54 cm square. A ball bearing, 0.7 cm in diameter was mounted on the shaft tip. The bonded PSA tape was attached face down in a rigid fixture. During the experiment, a mirror and a transparent ruler were used to observe the debond radius with a video camera (Figure 4). To account for the parallax error, a small correction was necessary. A schematic of the visual image as seen through the video camera is shown in Figure 5. The load (P) and displacement (w_0) were recorded by the universal testing machine (UTM), and the shaft displacement rate was 0.1 mm/s. The tests were conducted at room temperature. This

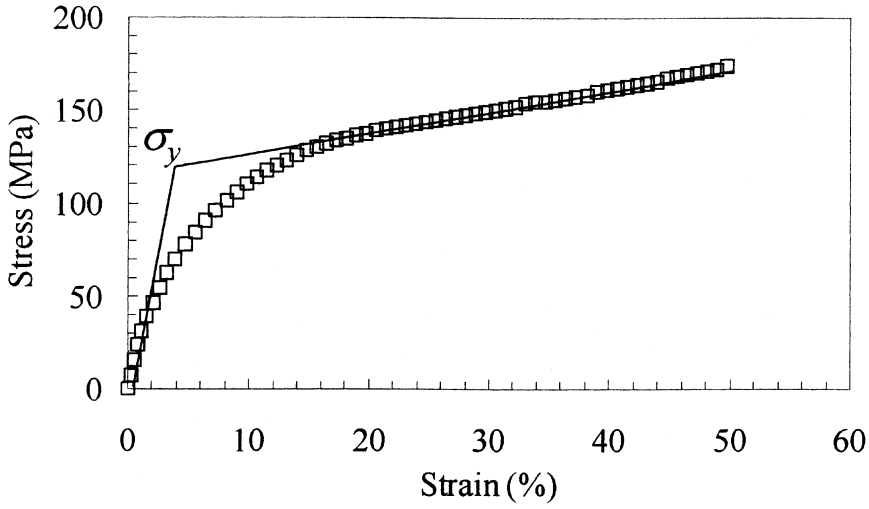

FIGURE 3 Stress-strain curve for Kapton®.

experiment is mechanically much simpler than the pressurized blister test since the mechanically driven shaft eliminates the use of a pump, pressure gauge, and valves. For the aluminum substrate, samples consisted of stacked, bonded, Kapton® PSA tape either 1, 2, or 4

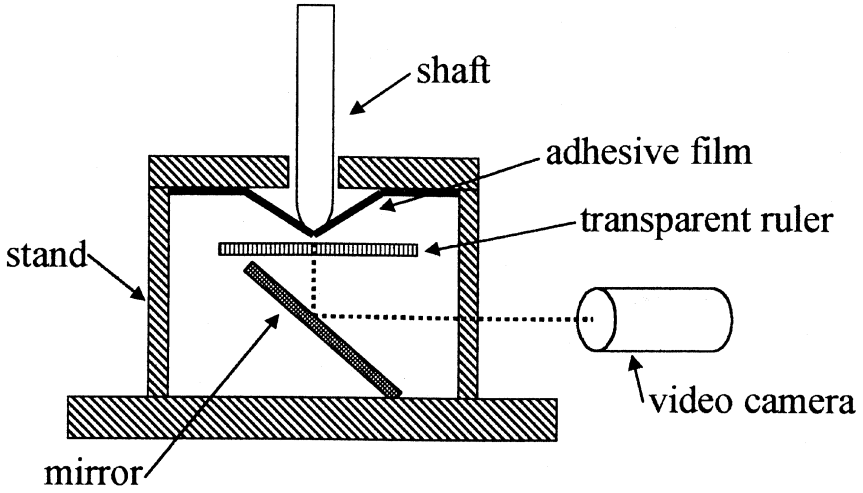

FIGURE 4 Schematic of the experimental set-up of the shaft-loaded blister test.

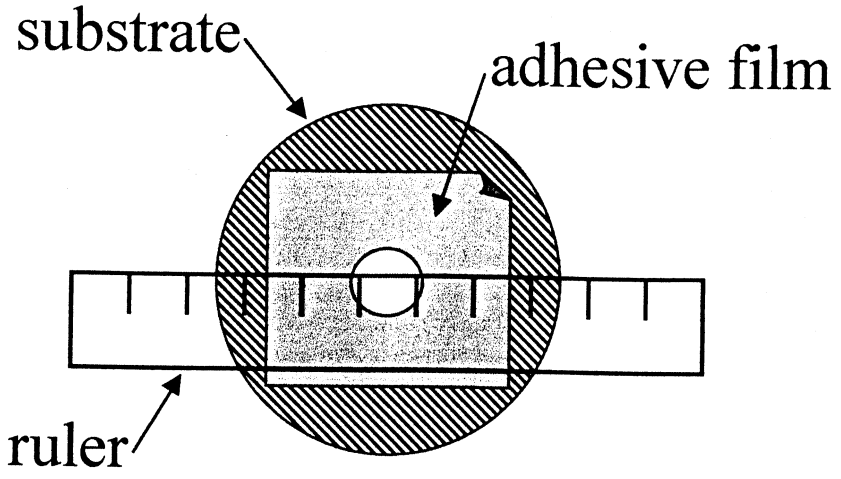

FIGURE 5 Schematic view of blister radius propagation.

plies thick. The number of stacked films is designated as n. As a result, the film thickness (h) based on the backing is equal to 25.4 μm multiplied by n. A single ply only was tested for the Teflon® substrate. The only criterion each sample must meet for acceptable analysis is that the debond must occur roughly axisymmetrically. For comparison, the strain energy release rate for a single ply of Kapton® tape was also measured by the pull-off test and the 90° peel test. For the pull-off test, G was calculated from Equation (2). For the 90° peel test, G was calculated from Equation (1), which in this case simplifies to Equation (8).

$$G = \frac{P}{b} \tag{8}$$

RESULTS AND DISCUSSION

Aluminum Substrate

Shaft-loaded blister test (SLBT)

The load (P) versus shaft displacement (w_0) curves obtained directly from the UTM are shown in Figure 6 for $n = 1$, 2, and 4. There are three regions of interest: Region I, the predebonding region at the beginning of the test where the blister begins to form; Region II, the stable crack growth region where the crack begins to propagate once a critical load (P^*) is reached and the slope of P versus w_0 becomes

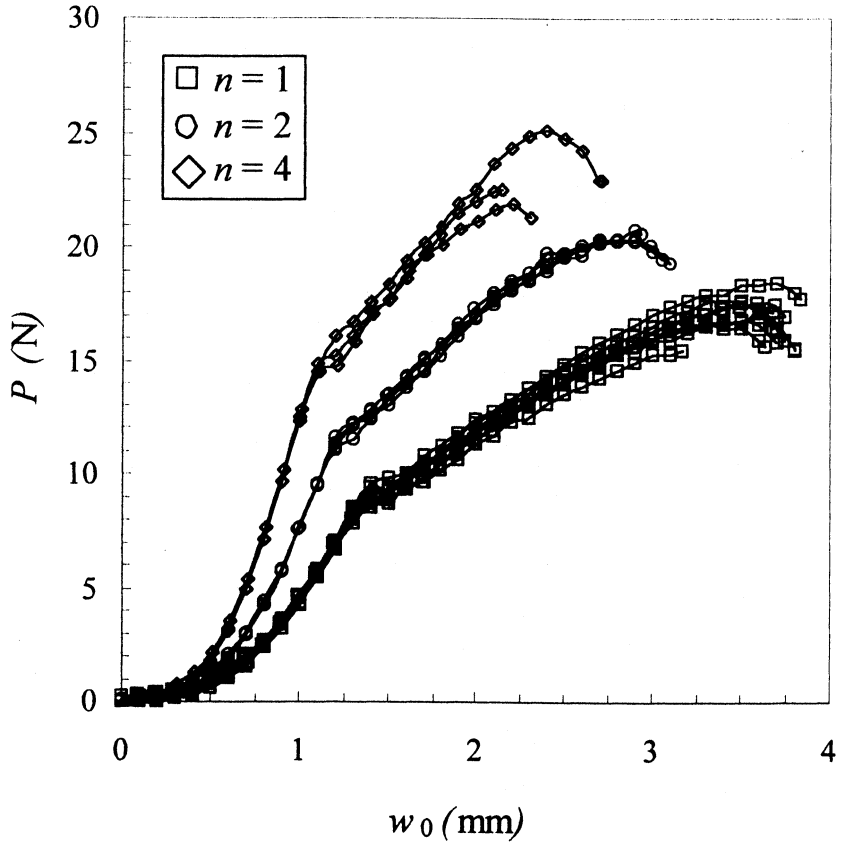

FIGURE 6 Load (P) *versus* central shaft displacement (w_0) for $n = 1$, 2, and 4.

linear; and Region III, where edge effects occur and the load begins to decrease as the film debonds completely from the substrate. From the slope of P versus w_0 in the stable crack growth Region II, the value of G may be determined using the hybrid equation (Equation (5)).

The debond radius (a) versus shaft displacement (w_0) data are shown in Figure 7 for $n = 1$, 2, and 4. From the slope of these lines, G may be determined using the displacement-based equation (Equation (6)). During stable crack growth the relationship of the load (P) and debound radius (a) is also linear, but it is not shown here. From the slope of the load (P) versus debond radius (a) plot, G may be determined using the load-based equation (Equation (4)). As mentioned by Wan and Mai [25], the nonzero intercept observed in Figures 6 and 7 are a result of the finite contact area between the shaft tip and adhesive film.

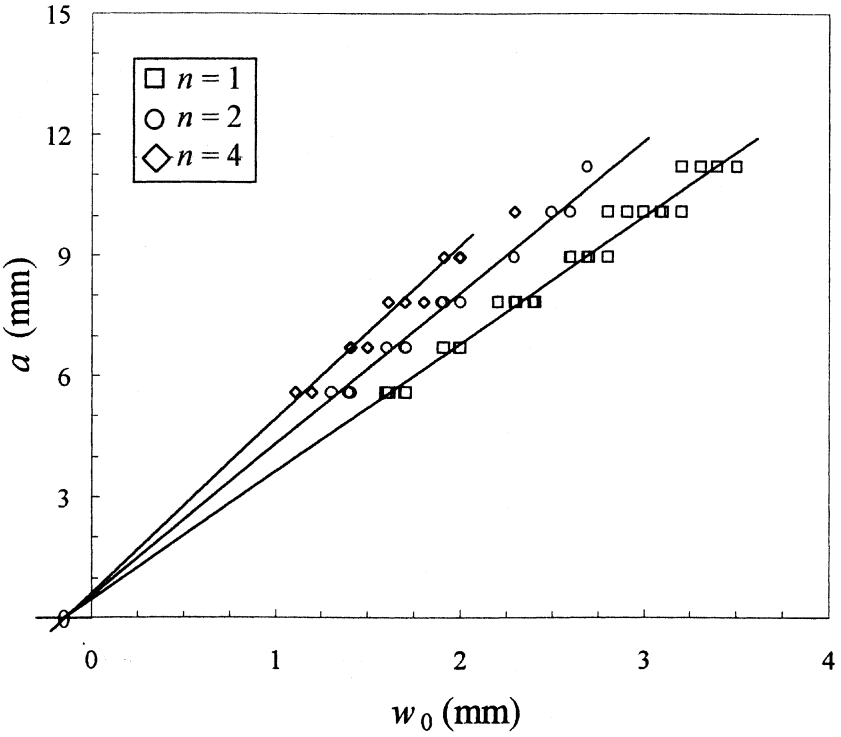

FIGURE 7 Debonding radius (a) versus central shaft displacement (w_0) for $n = 1$, 2, and 4.

For $n = 1$, 9 samples were tested. For the $n = 2$ and 4 specimens, we tested 4 and 3 samples, respectively, because fewer samples met the criterion of axisymmetric debonding. We noted that as the thickness increased, the debond radius tended to be less symmetric and the blister shape became roughly square, probably due to anisotropy in the film and to the increase in the stiffness of the film. This effect was most noticeable in the $n = 4$ case. Evidence for the anisotropy of the Kapton® backing can be found in an article by Park et al. [32].

Utilizing $(Eh)_{\mathrm{UTM}}$, the resulting calculated average values of G determined from the load-based, hybrid, and displacement-based equations are presented in Table 1 for $n = 1$, 2, and 4. For the load-based equation, the calculated values of G for different plies are in good agreement. The hybrid and displacement-based equations both show good agreement for $n = 1$ and $n = 2$ but not for $n = 4$. G values from the displacement-based calculation are significantly larger than those obtained by either the load-based or hybrid equation.

TABLE 1 Applied Strain Energy Release Rates (J/m^2) for $n = 1$, 2, and 4 on Aluminum Calculated from the Load-based, Hybrid, and Displacement Equations and $(Eh)_{UTM}$

n	Load (P/a)	Hybrid (P/w_0)	Displacement (w_0/a)
1	33.4 ± 3.6	31.9 ± 3.1	45.8 ± 10.4
2	35.0 ± 7.7	33.9 ± 5.2	44.8 ± 9.6
4	31.0 ± 2.2	24.2 ± 1.5	62.4 ± 11.1

The discrepancy between the values of G calculated by the load-based, hybrid, or displacement-based equations is largely associated with the (visible) plastic deformation at the contact zone between the shaft tip and PSA tape, where the stresses are highest. Equations (3)–(6) are based on an elastic, conical blister profile (Figure 2); however, the actual blister shape resembles that shown in Figure 8. As a result, the measured w_0 is larger than the theoretical, elastic w_0. This difference is especially significant in the displacement-based equation, where w_0 is in the numerator and is raised to the 4th power. Error in w_0 is less significant in the hybrid equation where w_0 is in the denominator and is raised to the 2nd power. As a consequence, the value of G determined from the displacement-based equation is significantly larger than the value of G calculated from the load-based or hybrid equation. In contrast, the value of G obtained by the load-based equation, having no w_0 term, is independent of plastic deformation of the film around the shaft tip.

A visible dimple remaining in the PSA tape at the contact region of the shaft tip after testing is evidence that significant localized plastic deformation or permanent set has occurred during testing. Additional evidence that significant permanent set has occurred was also gathered from the loading and unloading cycles, which were repeated

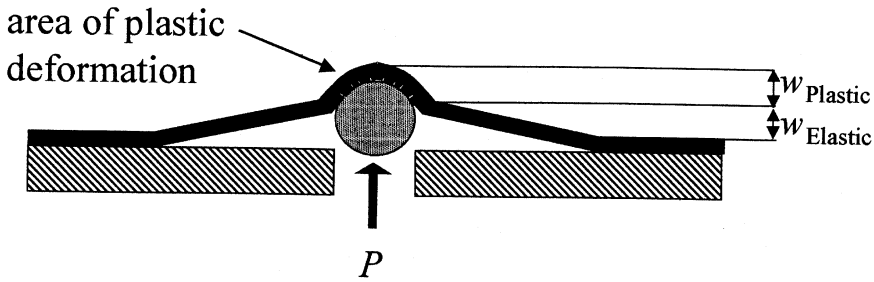

FIGURE 8 Schematic of the actual blister profile.

6 times. The area of contact between the shaft tip and adhesive film was coated with chalk to reduce effects of the adhesive film adhering to shaft tip. The substrate used for this experiment was polished aluminum, which is different from the aluminum treated with caustic solution that was used in the previous experiments. Although the adhesion strength is larger (≈ 71 J/m^2) for this substrate than that of the caustic solution-treated aluminum surfaces (≈ 35 J/m^2), the salient features of the loading and unloading cycles are most probably similar. Figure 9 displays the resulting graph of the load (P) versus displacement (w_0) for each cycle. Each cycle displays an initial loading region (Region I) followed by a brief zone of crack propagation (Region II) where the blister radius increased approximately 0.5–1 mm For each cycle, the characteristic signature of plastic deformation is evident where the displacement does not immediately return to the origin once the load is removed. Examination of Figure 9 shows that with each cycle there is a progressive increase in the amount of permanent set. The critical displacement (w_0), where the load first begins to rise,

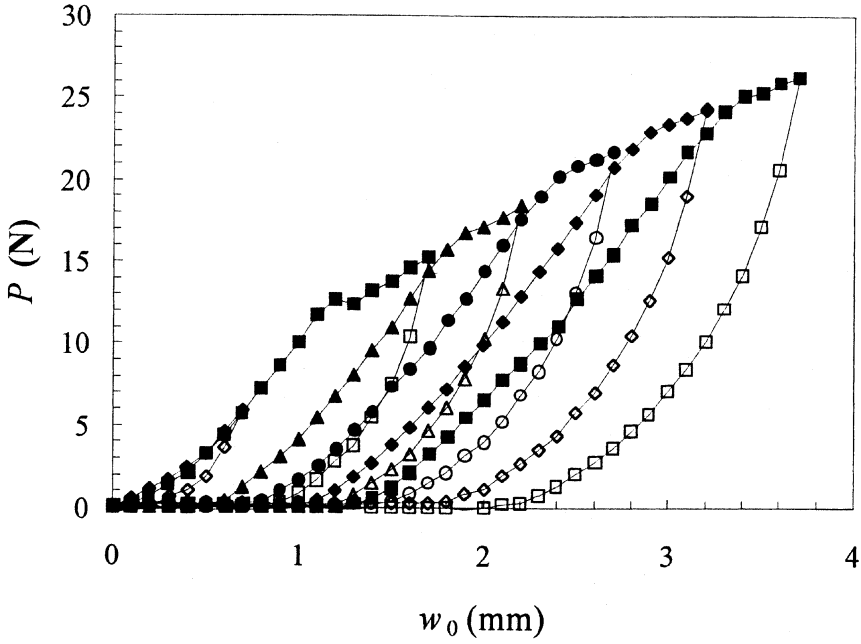

FIGURE 9 Loading and unloading cycles for Kapton® PSA tape bonded to polished aluminum. The loading portion of the curve is shown in filled symbols and the unloading portion is shown in unfilled symbols.

corresponding to the point where the shaft tip contacts the tape, increases with each subsequent cycle. However, during unloading, when the shaft tip returns to zero displacement, the PSA tape may partially readhere to the substrate. This can result in the load increasing prematurely. It is therefore more meaningful to look at the value of displacement when the load is completely removed as an indication of the permanent set that occurs. The final and maximum load (P_{Max}) of each cycle versus the displacement when the load is completely removed is shown in Figure 10. Figure 10 also shows that the net amount of film yielding increases with each subsequent loading cycle; however, the rate at which yielding increases slows. Taken collectively, the debonding regions (Region II) of each cycle appear to overlap in the same fashion as expected for a single P versus w_0 curve in which a specimen is loaded in a typical fashion.

The inaccurate value of w_0 (relative to the pure elastic case) and the resulting disagreement between the values of G, obtained by Equations (4), (5), and (6), may raise questions about the validity of the basic assumption of linear elasticity for the SLBT. To examine this, plots of N_{eff} versus r for different values of a were constructed as suggested by Equation (7) for $n = 1$, 2, and 4. As an example, the resulting plot for $n = 1$ is shown in Figure 11. We assume that if $N_{\text{eff}} \geq \sigma_p h$ then plastic deformation occurs. The resulting plots reveal

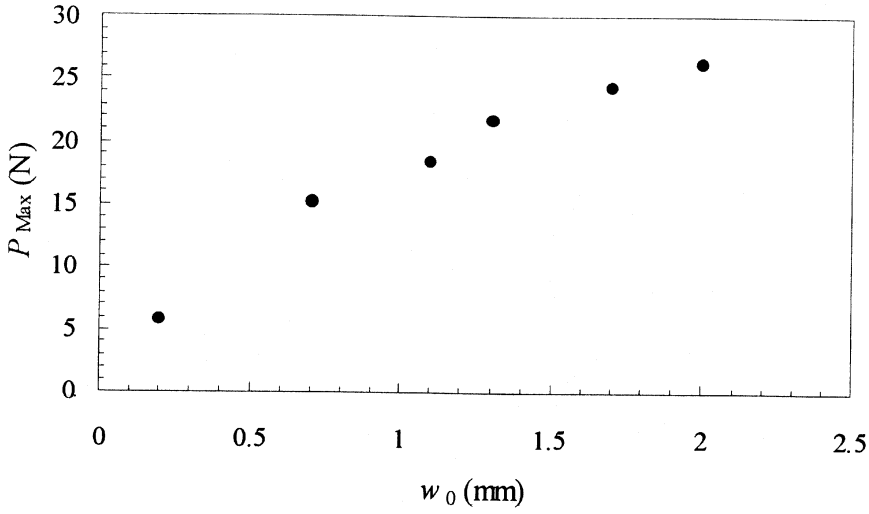

FIGURE 10 Plot of the final load, P_{Max}, of each cycle versus w_0 for Kapton® PSA tape bonded to polished aluminum.

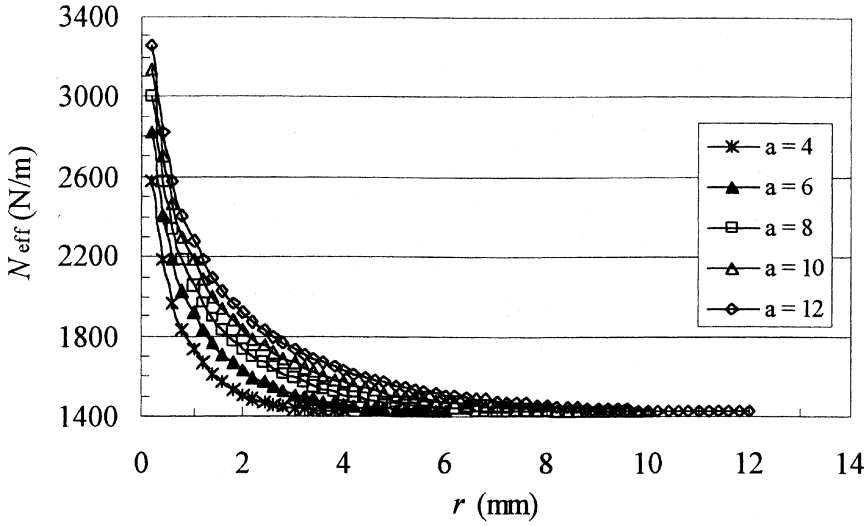

FIGURE 11 Plot of effective membrane stress as a function of crack length (a) and r.

that plastic deformation is predicted solely at the contact zone of the shaft tip ($r \leq 0.1$ mm for $n = 1$), and that no plastic deformation (attributable to radial and tangential stresses) is predicted to occur at the crack front ($r = a$). These results suggest that the assumption of linear elasticity is valid, if bending stresses are ignored.

Evidence of the adhesive-substrate system deviating from the assumptions of the model is observed for the multiple stacked tape, where $n = 4$. As shown earlier, the effects of plastic deformation here seem to be more pronounced; the value of G is either smaller or larger when calculated from the hybrid and displacement-based equation, respectively. This is unexpected, given that the stiffer film should plastically deform the least; therefore plastic deformation is probably not the most significant reason for the discrepancy. An alternative explanation is that for $n = 4$ the adhesive system does not follow the assumptions of the model as closely as in the $n = 1$ and $n = 2$ cases. The thicker structure should result in the adhesive behaving more like a bending plate and less like a stretching membrane. In addition, significant shear forces between the stacked plies are possibly playing a role. This shear effect may contribute significantly given that the four-layered structure of Kapton® is interspersed with the soft PSA and would reduce the effective stiffness of the film. As mentioned earlier, the deviation from the model is supported by the visual observation

that increasing the film stiffness and anisotropy may cause the blister to be less circular and to adopt a square or nonsymmetric debond pattern. However, when employing the load-based equation, the similarity between the $n = 4$ case and the model is close enough to obtain values of G close to those for to $n = 1$ and 2.

Rearrangement of the load-based, hybrid, and displacement-based equations shows that the slopes of the (P/a), (P/w_0), and (a/w_0) plots should linearly scale with the variables $h^{1/4}$, $h^{1/2}$, and $h^{1/4}$ or $n^{1/4}$, $n^{1/2}$, and $n^{1/4}$, respectively. Plots of such graphs using average slopes obtained from the group of samples are shown in Figure 12. The error bars represent one standard deviation. For the load-based equation, the predicted scaling behavior is followed, although the relationship is not perfect. For the hybrid and displacement-based equation, the graphs show that for $n = 4$ the scaling law fails, a result which may be attributable to reasons outlined previously.

The assumption of linear elasticity, and hence the validity of the model, is supported by calculations of N_{eff}. In addition, the agreement among the values of G obtained from the load-based equation for $n = 1$, 2, and 4 (independent of the film stiffness) is further evidence supporting the approach of Wan and Mai. It is not unexpected that the value of G obtained by hybrid and displacement-based equations do not agree with that obtained by the load-based equation, given the plastic deformation at the shaft tip unaccounted for by the elastic solution. If we accept that plastic deformation is confined to the area at the shaft tip, and linear elasticity is a valid assumption at the crack front $(r = a)$, then we can assume that the load and blister radius are in equilibrium and that the value of G obtained by the load-based equation is independent of film yielding near the shaft tip and provides good values of G. This is confirmed by the consistency of the values of G calculated using this method.

Alternative test geometries

The values of G for a single ply $(n = 1)$ PSA tape, which were obtained from alternative test geometries (the pull-off test and the 90° peel test), are shown in Table 2. The tests were performed at the identical crack propagation rate as that of the SLBT (10 mm/min) in order to reduce the viscoelastic differences at the crack tip. The value of G determined from the pull-off test was of the same order of magnitude as that obtained using the SLBT when employing the hybrid equation. The value of G determined from the 90° peel test was an order of magnitude greater than these, probably due to plastic deformation of the tape, which may originate from the bending stresses associated with the large angle of deflection between the peel arm and

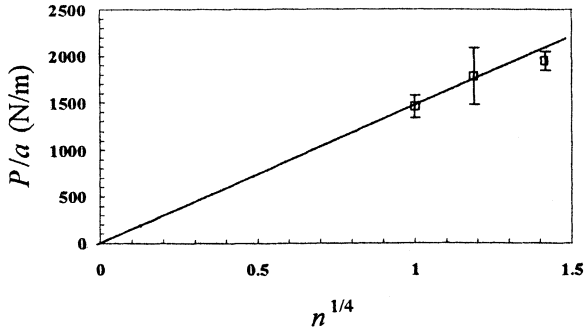

(a)

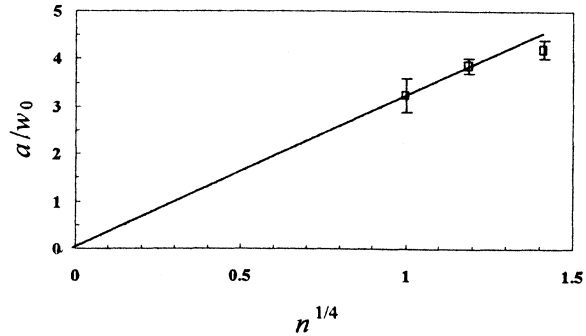

(b)

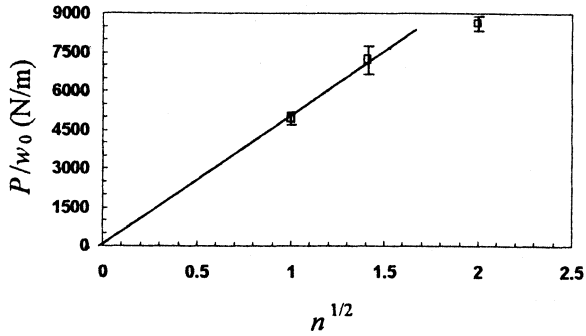

(c)

FIGURE 12 Plots of predicted scaling laws based on load, hybrid, and displacement equations.

TABLE 2 Applied Strain Energy Release Rates (J/m^2) Calculated from Alternative Test Geometries ($n = 1$)

Load-based SLBT	Pull-off test	90° Peel test
33 ± 4	45 ± 1	141 ± 7

substrate. These observations support our contention that the value of G obtained by the SLBT is a valid and especially attractive alternative to the 90° peel test. Similar to other low angle adhesion tests, the SLBT may produce values of G that more closely reflect the intrinsic adhesion strength of an adhesive system than do the high angle 90° and 180° peel counterparts. Both the pull-off test and SLBT share similar angles of debonding (for $n = 1$), roughly 14° and 16° (estimated from $\theta = arctan(w_0/a)$), respectively, and so large differences in the localized stress at the crack front are not expected. Although there may also be significant bending stresses associated with the SLBT given the similar angle of debonding between the SLBT and pull-off test, any bending stresses, if they are significant, may be similar in magnitude. The similarity between the pull-off test and SLBT, as well as how well established the pull-off test is, further supports the utility of the SLBT.

The assumption that the angle of debonding be less than 25°, used to derive the SLBT model, is satisfied. Furthermore, this angle appears to be constant given the linear relationship between the displacement (w_0) and debond radius (a). It is also of interest to mention that the SLBT, peel test, and pull-off test are all constant-angle adhesion tests, and so they share the characteristic of self-similarity and a value of G that is independent of the crack length or length of the peel arm.

Teflon® Substrate

Shaft-loaded blister test

Load (P) versus displacement (w_0), and crack length (a) versus displacement curves (w_0) were also generated for a single ply ($n = 1$) of the PSA adhering to a low surface energy Teflon® substrate, shown in Figure 13. Seven samples were tested. The resulting average values of G are listed in Table 3, there, as expected for such a low surface energy substrate, the values are low. Utilizing $(Eh)_{\mathrm{UTM}}$, the effects of plastic deformation are notable in this adhesive system; the average values of G obtained by the hybrid and displacement-based equations were

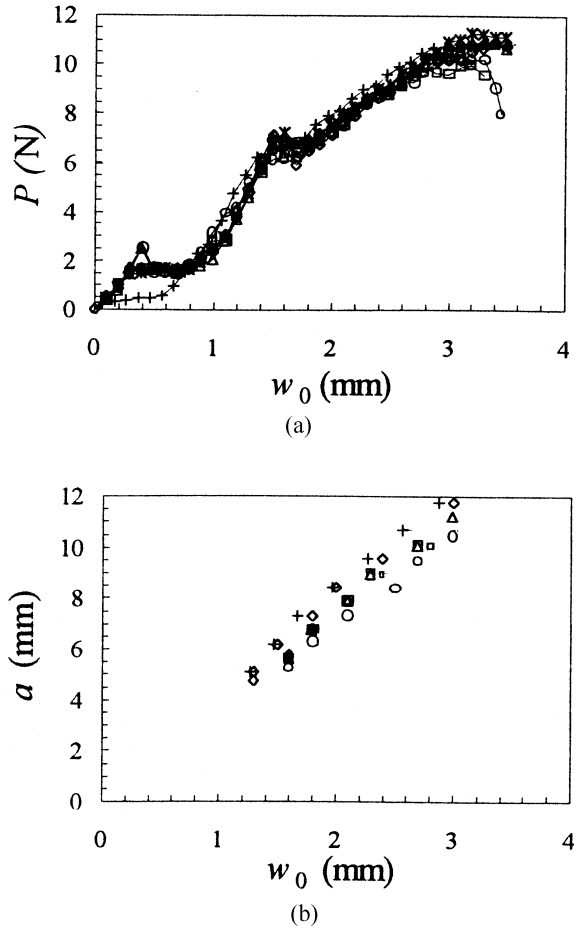

FIGURE 13 Load (P) versus central shaft displacement (w_0), and crack length (a) versus central shaft displacement curves (w_0), for Kapton® PSA tape bonded to Teflon ($n = 1$).

smaller and larger, respectively, relative to the load-based equation. However, the value of G calculated by the load-based and the hybrid equation agree within one standard deviation.

Alternative test geometries

The value of G obtained from the pull-off and 90° peel tests from Teflon®, with equal crack propagation rates, were approximately 60% greater than those found by the SLBT (Table 4). The agreement between the pull-off and 90° peel test is excellent. These results, in

TABLE 3 Applied Strain Energy Release Rates (J/m^2) for Kapton® PSA Tape Bonded to Teflon®, $n = 1$, Calculated from the Load, Hybrid, and Displacement Equations and $(Eh)_{UTM}$

Load (P/a)	Hybrid (P/w_0)	Displacement (w_0/a)
17.6 ± 3.4	15.5 ± 1.5	21.8 ± 4.2

conjunction with the values of G obtained by the pull-off test for aluminum, suggest that the fracture energies obtained by the SLBT will be slightly less than those obtained by the pull-off test. The agreement between the pull-off and 90° peel suggests that plastic deformation of the peel arm due to bending is reduced for the Teflon®–Kapton® combination. In sharp contrast, if the PSA tape is adhered strongly (*e.g.*, on the aluminum substrate), the bending of the peel arm causes significant plastic deformation when using the 90° peel geometry. Similar results were observed by Gent and Kaang [10] for adhesives with weak interfacial adhesion. More significant discrepancy could result as the yield strength of the film decreased or as the interfacial adhesion strength increased.

EFFECTS OF FLUIDS AT THE INTERFACE

The effect of fluid added directly to the interfacial region during crack propagation was investigated and is reported in terms of changes in the applied strain energy release rate. For these experiments, the reservoir between the PSA tape and aluminum substrate was filled with a mixture of methanol and water, and the load was immediately applied. The reservoir eliminates experimental difficulties associated with the complete fluid submersion of an adhesive specimen. The methanol concentration was varied from 0, 40, 60, 80, to 100 wt%. Tests were conducted at room temperature. A schematic of the experimental configuration is shown in Figure 14. The load (P) versus displacement (w_0) curves are shown in Figure 15. Table 5 lists the G values, calculated using the hybrid equation and the $(Eh)_{UTM}$, and

TABLE 4 Applied Strain Energy Release Rates (J/m^2) for Kapton® PSA Tape Bonded to Teflon®, $n = 1$, Using Alternative Test Geometries

Load based SLBT	Pull-off test	90° Peel test
18 ± 3	27 ± 1	26 ± 3

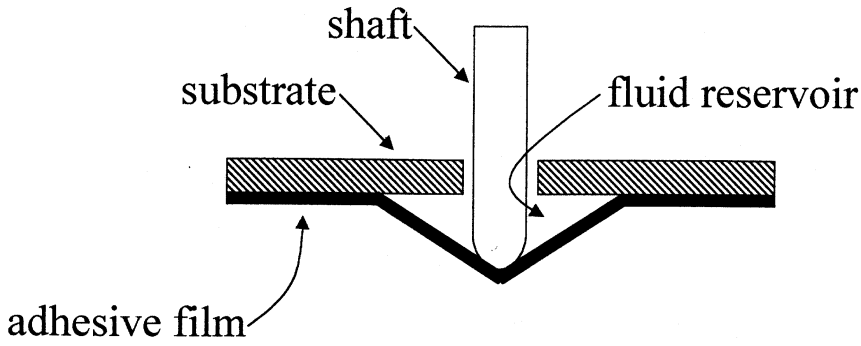

FIGURE 14 Schematic of the experimental set-up used to make *in situ* measure of liquid influence the strain energy release rate.

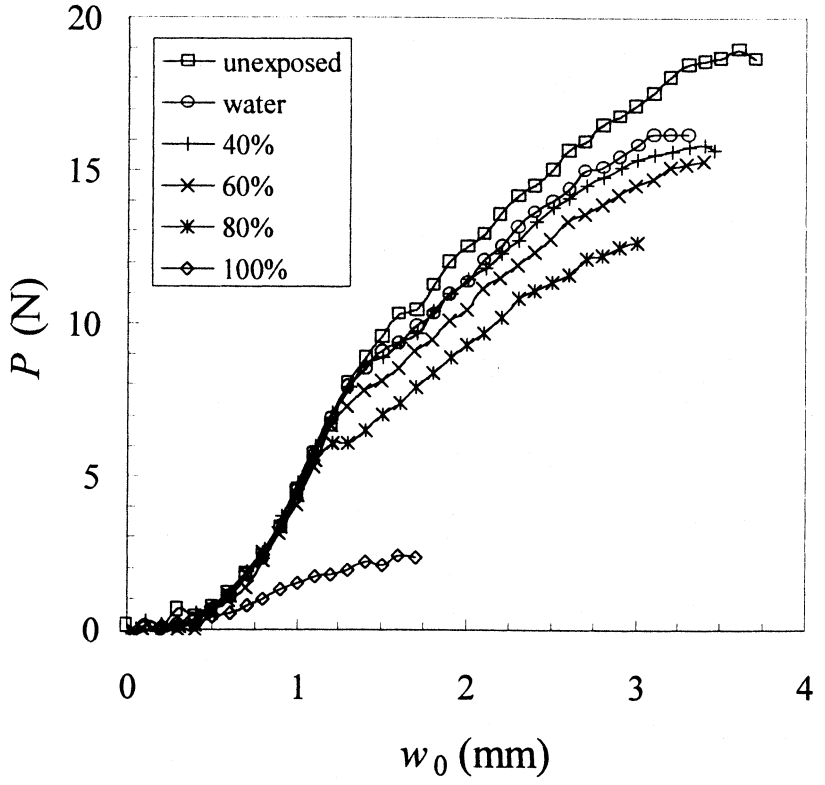

FIGURE 15 Load (P) versus central shaft displacement (w_0) for various concentrations of methanol in water (0, 40, 60, 80, and 100 wt%).

TABLE 5 Applied Strain Energy Release Rates (J/m^2) Calculated from Hybrid Equation for Kapton® Tape ($n = 1$) with Various Concentrations of Methanol in Water (0, 40, 60, 80, 100 wt%) and $(Eh)_{UTM}$

Methanol concentration	G (J/m^2)	P^* (N)
dry	36	9.6
0%	38.3	8.7
40%	31.6	8.7
60%	29.3	6.7
80%	27.8	5.2
100%	6.9	0.1

P^* for the respective methanol concentrations. Good agreement was noted between the value of G calculated from load-based and hybrid equations and $(Eh)_{UTM}$ for $n = 1$ and $n = 2$ bonded to aluminum. The presence of water (0% methanol concentration) increased the value of G, or at least within reasonable error did not have any measurable effect on the value of G. Furthermore, as the concentration of methanol increases, the critical load where debonding begins (P^*), and the slope of the P versus w_0 plot decreases.

Our results are similar to those obtained by Chaudhury and Whitesides [33] for the adhesion of PDMS surfaces in contact with mixtures of methanol and water. Utilizing the JKR model and Young's equation, they observed that the adhesion of PDMS surfaces in the presence of a high surface energy fluid ($\gamma = 72.94$ at 20°C [34]), water, was higher than in air. The work of adhesion for PDMS was determined to be 43.6 mJ/m^2 and 74 mJ/m^2 in air and in water, respectively. In the presence of a low surface energy fluid ($\gamma = 22.5$ at 20°C [34]), methanol, the adhesion of PDMS surfaces decreased to 6 mJ/m^2. The observed reduction in adhesion strength is attributable to the absorption of fluids on the surface; therefore, the lower the surface energy of the fluid, the more readily the fluid can wet the surface and disrupt the bonds between the adhesive and substrate.

CONCLUSIONS

We investigated the SLBT for its applicability in determining adhesive fracture energy of tapes adhering to rigid substrates. Plastic deformation at the contact area of the shaft tip resulted in an overestimated displacement, w_0 (relative to the elastic model), resulting in discrepancy among the values of G calculated by the load-based, hybrid, and displacement-based equations. Estimation of the effective mem-

brane stress (N_{eff}) in the film suggests that, in spite of the plastic deformation, the assumption of linear elasticity in the crack growth region and hence the validity of the model, seem reasonable.

As discussed in the Appendix, a compliance calibration has been adopted to measure $(Eh)_{\text{eff}}$, which agrees reasonably well with $(Eh)_{\text{UTM}}$ in cases of one or two plies of tape. For more layers of tape, the disagreement between $(Eh)_{\text{eff}}$ and $(Eh)_{\text{UTM}}$ is roughly 20% but is not unexpected given the large stiffness and the multilayered structure. The compliance calibration has been shown to improve the agreement between the value of G among the load-based, hybrid, and displacement-based equations; however, this appears to be an artifact of the error in w_0.

Using the load-based equation accurate values of G were obtained for a thin adhesive coating independent of the film's stiffness, even with plastic deformation at the shaft tip. The insensitivity of this load-based equation to the film stiffness suggests the compliance calibration is unnecessary. Comparing the value of G also obtained by a pull-off test and a 90° peel test for a single ply suggests that our value of G obtained by the SLBT, although of reasonable magnitude, is smaller than that obtained by the more firmly established pull-off test and also that the plastic deformation is reduced relative to the 90° peel test, presumably due to the low angle of deflection between the peel arm and substrate. An experimental configuration for studying the effects of liquids on the fracture energy has been demonstrated. This study indicates that the SLBT, because of the insensitivity of the load-based equation to the coating stiffness, the independence of the value of G on the plastic deformation at the shaft tip, and the reduced plastic deformation at the crack front relative to the 90° peel, is an attractive and convenient test method for measuring the strain energy release rate of adhesive films. Because the value of G is independent of the film stiffness, the SLBT could be advantageous for testing fragile thin films that could benefit from the addition of a reinforcement layer.

REFERENCES

[1] Lai, Y. H. and Dillard, D. A., *J. Adhesion Sci. Technol.*, **8**, 663–678 (1994).
[2] Kim, J., Kim, K. S. and Kim, Y. H., *J. Adhesion Sci. Technol.*, **3**, 175–187 (1989).
[3] Kendall, K., *J. of Physics D*, **4**, 1186–1195 (1971).
[4] Thouless, M. D. and Jensen, H. M., *J. Adhesion*, **38**, 185–197 (1992).
[5] Gent, A. N. and Kaang, S., *J. Adhesion*, **24**, 173–181 (1987).
[6] Gent, A. N. and Hamed, G. R., *J. Appl. Polym. Sci.*, **21**, 2817–2831 (1977).
[7] Kinloch, A. J., Lau, C. C. and Williams, J. G., *Int. J. Fracture*, **66**, 45–70 (1994).

[8] Moidu, A. K., Sinclair, A. N. and Spelt, J. K., *J. of Testing and Evaluation*, **23**, 241–253 (1995).
[9] Moidu, A. K., Sinclair, A. N. and Spelt, J. K., *J. of Testing and Evaluation*, **26**, 247–254 (1998).
[10] Gent, A. N. and Kaang, S., *J. Appl. Polym. Sci.*, **32**, 4689–4700 (1986).
[11] Wan, K. T., *J. Adhesion*, **70**, 197–207 (1999).
[12] Dannenburg, H., *J. Appl. Polym. Sci.*, **5**, 125–134 (1961).
[13] Williams, M. L., *J. Adhesion*, **4**, 307–332 (1972).
[14] Gent, A. N. and Lewandowski, L. H., *J. Appl. Polym. Sci.*, **33**, 1577–1597 (1987).
[15] Chang, Y. S., Lai, Y. H. and Dillard, D. A., *J. Adhesion*, **27**, 197–211 (1989).
[16] Napolitano, J., Chudnovsky, A. and Moet, A., *J. Adhesion Sci. Technol.*, **2**, 311–323 (1988).
[17] Allen, M. G. and Senturia, S. D., *J. Adhesion*, **25**, 303–315 (1988).
[18] Allen, M. G. and Senturia, S. D., *J. Adhesion*, **29**, 219–231 (1989).
[19] Dillard, D. A. and Bao, Y., *J. Adhesion*, **63**, 253–271 (1991).
[20] Wan, K. T. and Breach, C. D., *J. Adhesion*, **66**, 183–202 (1998).
[21] Wan, K. T., *Int. J. Adhesion & Adhesives*, **20**, 141–143 (2000).
[22] Tsunou, C., Sproat, E. A., Lai, Y. H., Shephard, N. E. and Dillard, D. A., *J. Adhesion*, **60**, 153–162 (1997).
[23] Moidu, A. K., Sinclair, A. N. and Spelt, J. K., *J. Adhesion*, **65**, 239–257 (1998).
[24] Malyshev, B. M. and Salganik, R. L., *Int. J. of Fracture Mechanics*, **1**, 114–128 (1965).
[25] Wan, K. T. and Mai, Y. W., *Int. J. of Fracture*, **74**, 181–197 (1995).
[26] Wan, K. T., DiPrima, A., Ye, L. and Mai, Y. W., *J. of Matl. Sci.*, **31**, 2109–2116 (1996).
[27] Wan, K. T., *J. Adhesion*, **70**, 209–219 (1999).
[28] Wan, K. T. and Liao, K., *Thin Solid Films*, **352**, 167–172 (1999).
[29] Blackman, B., Dear, J. P., Kinloch, A. J. and Osiyemi, S., *J. Mater. Sci. Lett.*, **10**, 253–256 (1991).
[30] Pocius, A. V., *Adhesion and Adhesives Technology: An Introduction* (Hanser/Gardner Publications, Inc., Cincinnati, Ohio, 1997) pp. 218.
[31] Kinloch, A. J., *Adhesion and Adhesives: Science and Technology* (Chapman and Hall, New York, 1987), pp. 26–34.
[32] Park, T., Dillard, D. A. and Ward, T. C., *J. Polym. Sci. Part B-Polym. Phys.*, **38**, 3222–3229 (2000).
[33] Chaudhury, M. K. and Whitesides, G. M., *Langmuir*, **7**, 1013–1025 (1991).
[34] Adamson, A. W., *Physical Chemistry of Surfaces* (John Wiley and Sons, Inc., New York, 1990), p. 41.

APPENDIX: EXPERIMENTAL COMPLIANCE CALIBRATION

Aluminum Substrate

An experimental compliance calibration was performed by fitting the experimental data to Equation (3). As predicted, the relation between Pa^2 *versus* ${w_0}^3$ (Figure 16) was linear and, from the slope of the line, the effective film tensile rigidity $(Eh)_{\text{eff}}$ was calculated. A comparison of this average $(Eh)_{\text{eff}}$ and the independently obtained $(Eh)_{\text{UTM}}$ is shown in Table 6. In all cases ($n = 1$, 2, and 4) the average $(Eh)_{\text{eff}}$ is less

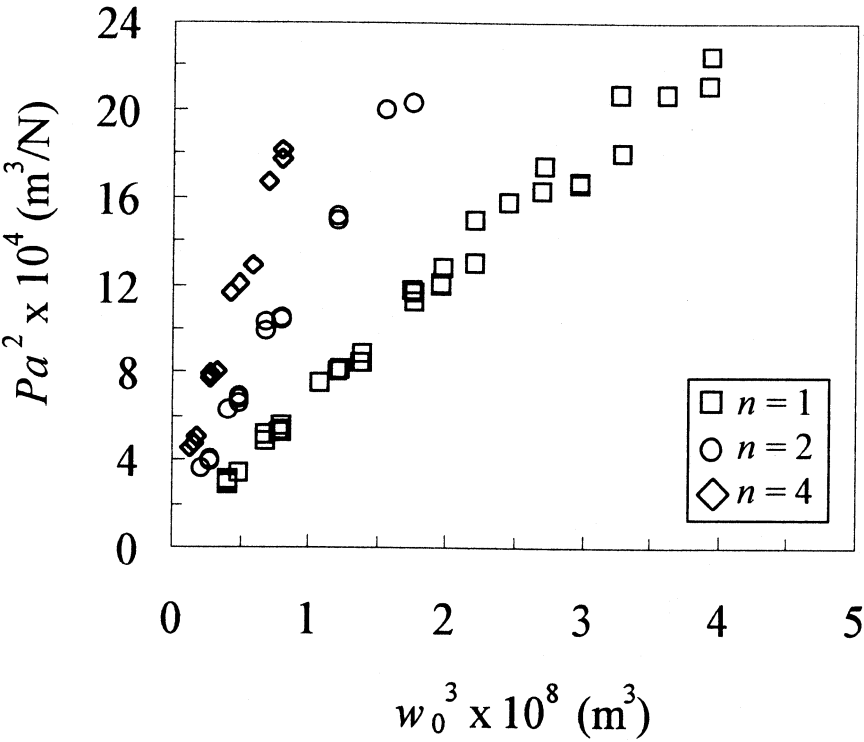

FIGURE 16 Linearized plot of Equation (7), Pa^2 versus w_0^3 for $n = 1$, 2, and 4.

than the $(Eh)_{\text{UTM}}$. For $n = 1$ the average $(Eh)_{\text{eff}}$ is about 9% less than $(Eh)_{\text{UTM}}$. The agreement is best for $n = 2$, the difference between the average $(Eh)_{\text{eff}}$ and $(Eh)_{\text{UTM}}$ being 3%. The disagreement between $(Eh)_{\text{UTM}}$ and $(Eh)_{\text{eff}}$ for $n = 4$, about 20%, is not unreasonable given the departure from the assumptions of the model of Wan and Mai, attributable to reasons discussed earlier: increased stiffness, anisotropy, and the multilayered structure.

TABLE 6 Film Tensile Rigidity Determined from ASTM D-882-91: $(Eh)_{\text{UTM}}$, and from Equation (3): $(Eh)_{\text{eff}}$, as Well as the Number of Samples Tested

n	$(Eh)_{\text{UTM}}$ N/m	$(Eh)_{\text{eff}}$ N/m
1	77,500	$70{,}600 \pm 6{,}300$
2	154,900	$150{,}800 \pm 11{,}600$
4	309,800	$252{,}100 \pm 17{,}200$

Utilizing $(Eh)_{\text{eff}}$, the average values of G determined from the load-based, hybrid, and displacement-based equations were calculated and are listed in Table 7 for $n = 1$, 2, and 4. Using $(Eh)_{\text{eff}}$, we note good agreement of G values between the load-based and hybrid equation (Table 3) irrespective of the number of plies. The disagreement observed when utilizing the displacement-based equation is attributed to the plastic deformation and was discussed earlier. A comparison of Tables 1 and 7 reveals no significant difference between the values of G measured using $(Eh)_{\text{UTM}}$ and $(Eh)_{\text{eff}}$. However, more consistency was obtained when the compliance calibration was utilized. When a compliance calibration was carried out for $n = 2$, virtually no difference in G values was observed, because of the small difference between $(Eh)_{\text{UTM}}$ and $(Eh)_{\text{eff}}$.

A larger value of w_0, relative to the purely elastic case, will affect the value of $(Eh)_{\text{eff}}$, obtained by fitting the experimental data to Equation (3). Examination of Equation (3) reveals that $(Eh)_{\text{eff}} \propto w_0^{-3}$. Therefore, the displacement w_0, which is overestimated if there is plastic deformation, would result in a calculated $(Eh)_{\text{eff}}$ which is less than that predicted in the case of a purely elastic response. However, the effects of plastic deformation and the multilayered structure of the PSA tape would also effectively reduce the stiffness of the film and contribute to the observation that $(Eh)_{\text{eff}}$ is less than $(Eh)_{\text{UTM}}$. The ambiguities associated with the discrepancy in w_0 are also exacerbated by the similar and strong dependence of the value of G on both w_0 and (Eh) in the hybrid and displacement-based equations. Examination of the hybrid equation and displacement-based equation reveals that $G \propto (Eh)^{-1} w_0^{-2}$, and $G \propto (Eh) w_0^4$, respectively. The load-based equation is less sensitive to the value of (Eh) relative to the hybrid and displacement-based equation because $G \propto (Eh)^{-1/3}$. Because of the relative difference between the values of $(Eh)_{\text{eff}}$ and $(Eh)_{\text{UTM}}$, utilizing $(Eh)_{\text{eff}}$ rather than $(Eh)_{\text{UTM}}$ resulted in increasing the value of G obtained by the hybrid equation and decreasing the value of G obtained by the displacement-based equation. The net effect is that the

TABLE 7 Applied Strain Energy Release Rates (J/m^2) for $n = 1$, 2, and 4 on Aluminum Calculated from the Load, Hybrid, and Displacement Equations and the Effective Tensile Rigidity $(Eh)_{\text{eff}}$

n	Load (P/a)	Hybrid (P/w_0)	Displacement (w_0/a)
1	34.7 ± 4.2	35.1 ± 4.5	40.7 ± 6.9
2	35.3 ± 7.7	34.7 ± 2.9	43.5 ± 9.3
4	33.3 ± 2.9	29.8 ± 2.7	50.3 ± 5.4

TABLE 8 Applied Strain Energy Release Rates (J/m^2) for Kapton® PSA Tape Bonded to Teflon®, $n = 1$, Calculated from the Load, Hybrid, and Displacement Equations and the Effective Modulus $(Eh)_{eff}$

Load (P/a)	Hybrid (P/w_0)	Displacement (w_0/a)
18.7 ± 3.6	18.6 ± 1.5	18.2 ± 4.2

apparent results of plastic deformation are offset by a corresponding reduction in the value of (Eh). This produced more consistent results when $(Eh)_{eff}$ was incorporated into the calculations. This might lead to the conclusion that $(Eh)_{eff}$ better describes the stiffness of the film and more closely reflects the mechanical propeties of the film in the SLBT loading conditions as compared with $(Eh)_{UTM}$. However, given the dependency on the overestimated displacement, it is unlikely that the value of $(Eh)_{eff}$ truly reflects the mechanical properties of the film loaded in the SLBT geometry, but is an artifact of the error in w_0. In any case, the linear fit of the experimental data to Equation (3), and the reasonable agreement between $(Eh)_{eff}$ and $(Eh)_{UTM}$ (especially for $n = 2$) support the validity of Wan's model and the assumption of linear elasticity.

Teflon® Substrate

By fitting the experimental data to Equation (3) an average $(Eh)_{eff}$ was calculated as $64{,}700 \pm 7{,}100$ N/m, approximately 17% less than $(Eh)_{UTM}$. Using the experimental compliance calibration, the average value of G was in good agreement among all three equations (Table 8). Again, this is probably a result of the strong dependence of G on both (Eh) and w_0 for the hybrid and displacement equation; or, it could be that $(Eh)_{eff}$ more closely reflects the mechanical properties of the adhesive loaded in the SLBT conditions. If indeed $(Eh)_{eff}$ is reasonable, the good agreement would not be unexpected given that the Teflon®–PSA system complies well with the assumptions of the model: namely, (1) the reduced bending stresses attributable to the small thickness (single ply), and (2) the reduced interfacial adhesion strength, which reduces stress and/or plastic deformation in the adhesive.